A Numerical Model for the Transport of Chromium and Fine Sediments

Alfredo Emilio Trento & Ana M. Alvarez

Environmental Modeling & Assessment

ISSN 1420-2026
Volume 16
Number 6

Environ Model Assess (2011) 16:551-564
DOI 10.1007/s10666-011-9263-5

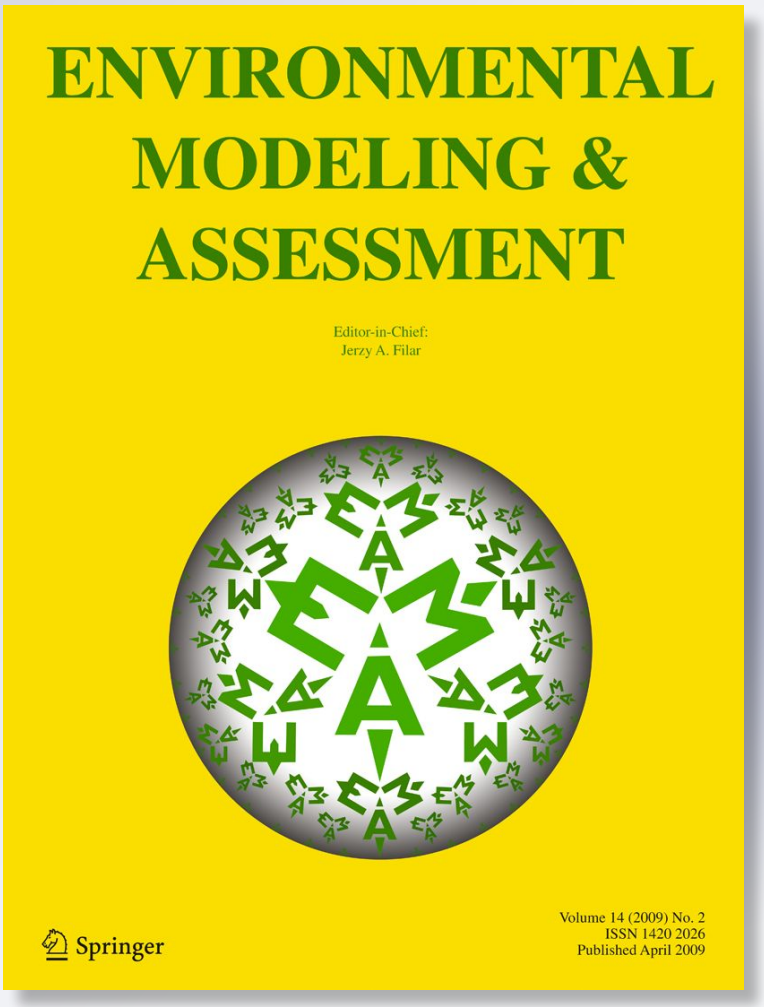

Springer

Environ Model Assess (2011) 16:551–564
DOI 10.1007/s10666-011-9263-5

A Numerical Model for the Transport of Chromium and Fine Sediments

Alfredo Emilio Trento · Ana M. Alvarez

Received: 5 March 2008 / Accepted: 6 May 2011 / Published online: 24 May 2011

Abstract A mathematical model which represents the transport processes of heavy metals and fine sediments in a fluvial stream was developed. The model consists of a three-equation system: the first one for total chromium concentration in the water column, C_{Tw}, the second one for total suspended sediment concentration, S_w, and the third one for chromium concentration in bed sediments, r. The third equation represents the chromium exchange between the water column and bed sediments by two processes: diffusion of soluble chromium and erosion/deposition of chromium sorbed to sediments. The basic assumption of the model is the instantaneous equilibrium. The main parameters are the partition coefficients in the water column and bed sediments, the depth of the active bed sediment layer, and the mass transfer coefficient between the water column and sediment pore water. The numerical model approximates the equations of advection–dispersion for chromium in water and suspended sediments by using a Eulerian third-order scheme. Numerical vs. analytical solutions were considered satisfactory for different initial, boundary, and sedimentological conditions. In order to estimate the impact of a chromium side discharge, the model was implemented for the Salado River in a reach of 65.6-km long (Santa Fe, Argentina). The results showed the effect of chromium discharge on almost the whole reach, then the vulnerability of the water quality in the Salado River when the flow was low was evidenced. When comparing the computed and measured results, the former showed a reasonable representation of the presence of chromium in water and bed sediments.

Keywords Sediment · Partition · Chromium · Salado River

A. E. Trento (✉) · A. M. Alvarez
Facultad de Ingeniería y Ciencias Hídricas,
Universidad Nacional del Litoral,
Ciudad Universitaria, CC 217,
3000, Santa Fe, Argentina
e-mail: alfredotrento@yahoo.com
e-mail: atrento@fich.unl.edu.ar

A. M. Alvarez
e-mail: aalvarez@fich.unl.edu.ar

1 Introduction

Heavy metals (HM) such as chromium from natural or anthropogenic origin are chemical substances that undergo complex biogeochemical cycles. HM do not degrade in the environment [38] and are persistent and toxic under certain conditions [2, 29]. They are distributed between two phases: the dissolved and the particulate phases, in aquatic ecosystems, e.g., lakes, rivers, and coastal areas. The first one refers to the water column and the sediment pore water; the second one, the particulate phase, refers to the HM adsorbed on suspended and bed sediments.

It is worth noting that the sediments are an integral and inseparable part of a river [41], which serve as sinks of HM and may be transported into streams, plains, and estuaries [13, 40, 59]. These sediments may eventually become a potential source of contamination by processes of erosion/resuspension [55]. In addition, they hold up to a million times more metal than an equivalent volume of water, being this proportion a function of the chemistry of the metal, the sediment, and the surrounding environment [9]. Particularly, it is believed that fine sediments, such as silts and clays, of an aquatic system are of extreme importance in the HM transport [31] due to their high surface area and their physicochemical properties of adsorbing substances [27].

Several international environmental organizations consider sediment contamination as a major risk in aquatic environments because HM remain in the medium as micropollutants of high toxicity [47, 48].

Among several HM, chromium in its +3 and +6 oxidation states, is of a major concern because it could be accumulated by several aquatic vegetation species, which in turn may be consumed by herbivorous fish [23]. Furthermore, human beings could also be affected by this metal from direct ingestion of contaminated fish or from ingestion of food which had been in contact with contaminated water for a considerable time [4].

The study of the transport processes of chromium association with sediments was carried out, at laboratory scale, by Turner and Millward [44], Turner [46], USEPA [49, 50], Wen and Allen [53], and Jackman et al. [17] while Wang and Chen [52] and Karvelas et al. [21] focused on the statistical analysis of those processes. A complete conceptual and mathematical formulation for HM and sediment transport processes in riverine and estuarine environments was developed by Schnoor [38] and Chapra [6], among others. Each author proposed a system of partial differential equations to represent the main mechanisms governing the interaction of chromium, between the dissolved and particulate phases, both in the water column as well as in the bed. Over the past two decades, several numerical models were developed to simulate the dynamics of metals and sediments in aquatic environments, using one-dimensional (1D) cross-sectional averaged model [18, 58], two-dimensional (2D) depth averaged [7, 22, 30, 39, 58], two-dimensional laterally averaged [54], three-dimensional (3D) numerical models [14, 15, 34, 37], or a combination of 1D and 2DH models [57]. Although the fully 3D and 2D models were often used, the 1D models are efficient and economical tools to study hydro-environmental dynamics in a 1D view of rivers. For many engineering problems, the one-directional physical features are prevalent in many riverine waters. This is the case of the Salado River, where the length of the reach of interest is over tenfold its width.

The aim of this study was to develop and implement an Eulerian numerical model to simulate the nonsteady transport of chromium in water, bed sediments, and fine suspended sediments in a fluvial watercourse.

The model was implemented in a reach 65.6-km long of the Salado River, the Cululú Stream and the 1° de Mayo Channel (Santa Fe Province), where there is a chromium side discharge to the Salado River.

2 Conceptual Model

The dissolved HM in the water column are transported by the advection and dispersion processes, while the HM in the particulate phase are governed by sediment dynamics. HM behavior in water bodies is strongly influenced by sorption kinetics. If the adsorption and desorption processes are fast compared to advection, dispersion, erosion/resuspension, and deposition processes, then an assumption of instantaneous equilibrium may be used [15, 38]. Therefore, solid concentrations in the water column must be constant or must change slowly along the stream. Generally, sorption kinetics is fast compared to the HM transport processes [16, 60], except perhaps along effluent dispersion plume [12] or immediately following a pulse exposure, such as an overflow from a storm sewer system [9].

The partition or distribution coefficients in the water column $\mathrm{Kp_w}$ [cubic meter per kilogram] and bed $\mathrm{Kp_b}$ [cubic meter per kilogram] are defined by Thomann and Mueller [43] as the ratio between the metal mass (normalized to dry solid mass) and the metal concentration in the solution. The $\mathrm{Kp_w}$ and $\mathrm{Kp_b}$ coefficients depend on the physical and chemical features of the suspended sediments as well as various environmental conditions, such as pH, salinity, redox potential, and dissolved organic matter content [20, 44]. $\mathrm{Kp_w}$ is:

$$\mathrm{Kp_w} = \frac{C_{\mathrm{pw}}}{C_{\mathrm{sw}}\, S_{\mathrm{w}}} \tag{1}$$

where C_{sw} and C_{pw} are the concentrations [kilogram HM per cubic meter] of soluble and particulate metal in water and S_{w} is the solids concentration in the water column [kilogram per cubic meter]; s indicates soluble, p, particulate, and w, water. Corresponding units are expressed between square brackets, being $\mathrm{kg_{HM}}$ and kg, HM and sediment concentration masses. $\mathrm{Kp_b}$ is expressed as follows:

$$\mathrm{Kp_b} = \frac{C_{\mathrm{pb}}}{C_{\mathrm{sb}}\, S_{\mathrm{b}}} = r/C_{\mathrm{sb}} \tag{2}$$

where C_{sb} and C_{pb} are the concentrations [kilogram HM per cubic meter] of soluble and particulate metal in the bed, and S_{b} is the [kilogram per cubic meter] sediment concentration in the bed environmental volume. r [kilogram HM per kilogram] is the concentration of HM sorbed in bed sediments. S_{b} is expressed according to bed porosity, ϕ, as $S_{\mathrm{b}} = \rho_{\mathrm{s}}(1-\phi)$, and ρ_{s}=2,650 kg $\mathrm{m^{-3}}$ is the mass density of the sediment grains. Figure 1 shows the processes and mechanisms governing the HM cycle in an aquatic environment, both in the water column of h depth and in the depth of the active bed sediment layer, d_{a}. The latter represents the vertical spatial scale of the HM penetration in the bed sediments, which is measured from the water–bed interphase and is assumed to be constant. Moreover, HM (chromium) concentration in d_{a} is also assumed to be homogeneous. The velocity at which dissolved HM moves vertically in the bed sediments through d_{a} is denoted by k_{L} [meter per second]

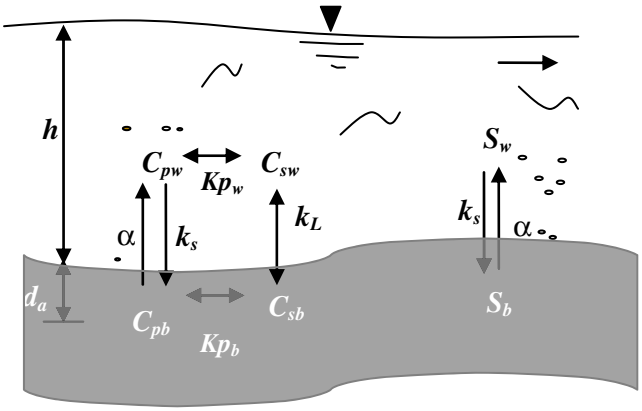

Fig. 1 Scheme of processes and mechanisms governing the heavy metal cycle in an aquatic environment (adapted from Schnoor 1996). C_{sw} concentration of soluble metal in water, C_{pw} concentration of particulate metal in water, C_{sb} concentration of soluble metal in bed sediments, C_{pb} concentration of particulate metal in bed sediments, S_w solids concentration in the water column, S_b sediment concentration in the bed environmental volume, k_s deposition rate, α the resuspension or erosion rate, k_L mass transfer coefficient between water column and pore water of bed sediments, d_a active bed sediment layer, h depth of water column

coefficient. This mass transfer process of dissolved HM occurs by means of a diffusive process, according to Fick's law. Di Toro [8] suggests using a coefficient of average molecular diffusion, D, in order to compute $d_a = D/k_L$. Also, the deposition rate, k_s [per second], and the resuspension or erosion rate, α [per second] are considered. The presence and evolution of bed forms, e.g., dunes, do not change d_a or S_b because the spatial and temporal scales of their displacement in shallow waters are negligible compared with HM and suspended sediment transport scales.

The sorption of chromium can occur in the particles of suspended solids or flocs. If cohesive sediments, clay, and fine silt are present, then all or a portion of the suspended fine sediments (<63 μm) can be flocculated [24, 28]. Therefore, the dynamics of sedimentation will be governed by the size and density of flocs, with a different sedimentation mechanism from the thousands of particles that compose them [56]. The flocculation process will not be considered in the present work, then a reference value for the settling velocity, W_s [meter per second], is adopted. Bioturbation caused by the activity of the benthic fauna, which can increase porosity, will not be considered [36].

3 Mathematical Model for the Transport of Heavy Metals and Fine Sediments in Rivers

Schnoor [38] proposed a mathematical model of six differential equations in partial derivatives (DEPD), following the conceptual model (Fig. 1). Two equations describe chromium soluble and particulate transport in the water column, as a function of C_{sw} and C_{pw}. Other two DEPD describe chromium soluble and particulate transport in bed sediments, as a function of C_{sb} and C_{pb}, and the last two equations correspond to the concentrations of suspended sediments and bed sediments, S_w and S_b. If the instantaneous local equilibrium assumption is considered for the sorption process, the Schnoor model can be reduced to just two DEPD, for the dependent variables C_{Tw} and r. However, when spatial and temporal changes of S_w are slow, a third equation is regularly used in HM transport models, e.g., [7, 15, 18, 32, 33, 39, 57]. Therefore, the first equation represents the total concentration of chromium in water, $C_{Tw} = C_{sw} + C_{pw}$, the second one represents the chromium concentration sorbed in bed sediments, r, and the third one represents fine suspended solid concentrations, S_w:

$$\frac{\partial C_{Tw}}{\partial t} = -\frac{1}{A}\frac{\partial}{\partial x}(UAC_{Tw}) + \frac{1}{A}\frac{\partial}{\partial x}\left(D_L A \frac{\partial C_{Tw}}{\partial x}\right) + \frac{k_L}{h}\left(\frac{r}{Kp_b} - \frac{C_{Tw}}{1 + Kp_w S_w}\right) + \alpha\frac{rS_b}{\gamma} - k_S\frac{C_{Tw}Kp_w S_w}{1 + Kp_w S_w} \tag{3}$$

advection | dispersion | pore − water − diffusion | erosion | deposition

$$\frac{\partial r}{\partial t} = -\frac{k_L}{d}\frac{\left(\frac{r}{Kp_b} - \frac{C_{Tw}}{1+Kp_w S_w}\right)}{\frac{1}{Kp_b} + S_b} + k_s\frac{\gamma C_{Tw}\frac{Kp_w S_w}{1+Kp_w S_w}}{\frac{1}{Kp_b} + S_b} - \alpha\frac{r S_b}{\frac{1}{Kp_b} + S_b} \tag{4}$$

pore − water − diffusion | deposition | erosion

$$\frac{\partial S_w}{\partial t} = -\frac{1}{A}\frac{\partial(UAS_w)}{\partial x} + \frac{1}{A}\frac{\partial}{\partial x}\left(D_L A\frac{\partial S_w}{\partial x}\right) + \frac{1}{h}(m_e - m_d) \tag{5}$$

advection | dispersion | erosion − deposition

where U is the mean velocity in the cross section [meter per second], A is the area of the cross section [square meter], D_L is the longitudinal dispersion coefficient [square meter per second], x is the longitudinal coordinate [meter], and t is the temporal coordinate [seconds], m_e and m_d [kilogram per square meter per second] are erosion and deposition rates, respectively. $\gamma = h/d_a$ is a dimensionless coefficient which represents the geometrical scale of the depth with respect to the active layer. The first term on the right of Eq. 3 represents advective transport of chromium, the second term represents transport resulting from dispersion,

the third one corresponds to HM transfer between the water column and sediment pore water by diffusion. The fourth term represents the chromium incorporated to the water column from the bed sediment by erosion. The fifth term is chromium loss from the water column by sediment deposition. As to Eq. 4, the terms on the right are analogous to the last three terms of Eq. 3. The sign of the first term of Eq. 4 can be positive or negative, according to the ratio $(r/\mathrm{Kp_b} - C_{\mathrm{Tw}}/(1+\mathrm{Kp_w}\ S_\mathrm{w})$ which is equivalent to $(C_{\mathrm{sb}} - C_{\mathrm{sw}})$. When $C_{\mathrm{sb}} > C_{\mathrm{sw}}$ there will be an addition of chromium to the water column by diffusion from the bed. In the opposite case, when $C_{\mathrm{sb}} < C_{\mathrm{sw}}$, there will be an increase of chromium in the bed at the expense of the dissolved chromium in the water column. Remarkably, this process in either direction is independent of the erosion/deposition relationship.

The first and second terms on the right of Eq. 5 correspond to the fine sediment transport by advection and dispersion, respectively. The third one represents the fine sediment balance in the water column by erosion and deposition processes.

The main parameters of erosion and deposition processes are: the critical shear stress, τ_e, and the critical velocity for sediment deposition, U_{cr}, respectively. The erosion rate can be expressed as follows [1]:

$$m_\mathrm{e} = E_\mathrm{e}\left(\frac{\tau_\mathrm{b}}{\tau_\mathrm{e}} - 1\right) \quad \text{when } \tau_\mathrm{b} > \tau_\mathrm{e}, \tag{6}$$

where E_e [kilogram per square meter per second] is an empirical constant, whose units correspond to those of m_e and $\tau_\mathrm{b} = \rho_\mathrm{w}\ u_*^2$ is local shear stress, with ρ_w water density, u_* friction velocity, $u_* = Ung^{0.5}R^{-1/6}$, n is the Manning coefficient, g gravitational acceleration, and R hydraulic radius. When $\tau_\mathrm{b} < \tau_\mathrm{e}$, then $m_\mathrm{e}=0$. As to deposition, Nicholas et al. [35] postulated the deposition rate of suspended solids as:

$$m_\mathrm{d} = S_\mathrm{w}\left\{\lambda\ W_\mathrm{s}\left[1 - \left(\frac{U}{U_{\mathrm{cr}}}\right)^2\right] + q\,p\,E\right\} \tag{7}$$

where λ is a dimensionless empirical constant, q [square meter per second] is floodplain unit flow in the x direction, p is the proportion of the water column occupied by vegetation, and E is the vegetation trapping efficiency per unit distance. The first term in Eq. 7 represents deposition due to particle settling when $U < U_{\mathrm{cr}}$. The second term represents sediment entrapment for vegetation, and it is relevant for floodplain deposition. If there is no floodplain flow, then $q=0$. By comparing the erosion terms in Eqs. 3, 5, and 6, the relationship between α and E_e can be obtained:

$$\alpha = \frac{E_\mathrm{e}}{d_\mathrm{a}\,S_\mathrm{b}}\left(\frac{\tau_\mathrm{b}}{\tau_\mathrm{e}} - 1\right) \tag{8}$$

Then by analyzing the deposition terms in Eqs. 5 and 7, and Schnoor [38] definition, $k_\mathrm{s}\ S_\mathrm{w} = m_\mathrm{d}/h$, what is obtained for k_s is, as follows:

$$k_\mathrm{s} = \frac{\lambda\ W_\mathrm{s}}{h}\left[1 - \left(\frac{U}{U_{\mathrm{cr}}}\right)^2\right] \tag{9}$$

Therefore, the formula $k_\mathrm{s} = W_\mathrm{s}/h$ [38] should be considered just an approximation.

4 Numerical Model

The governing Eqs. 3 and 5 were resolved by means of a Eulerian numerical scheme which makes possible the representation of spatial and temporal variations of C_{Tw} and S_w. The model is based on the well-known Quickest scheme proposed by Leonard [26], which presents a spatial and temporal third-order truncation error and has practically no oscillations of the centered schemes and no numerical dissipation of the regressive schemes, even under advective conditions. The calculation is updated at each computational time step Δt, while hydrodynamic variables of gradually varied unsteady flow, U and h, are updated at longer time intervals. Equation 3 is then discretized as follows:

$$C_{\mathrm{Tw}_j}^{t+1} = C_{\mathrm{Tw}_j}^t + \frac{1}{A_j}\left(a_{1_{j+1}}\,C_{\mathrm{Tw}_{j+1}}^t + a_{2_j}\,C_{\mathrm{Tw}_j}^t + a_{3_{j-1}}\,C_{\mathrm{Tw}_{j-1}}^t + a_{4_{j-2}}\,C_{\mathrm{Tw}_{j-2}}^t\right) - a_{5_j}\,C_{\mathrm{Tw}_j}^t + a_{6_j}\,r_j^t \tag{10}$$

$$a_{1_{j+1}} = A_{j+1}\left(\Gamma\left(1 - c_j\right) - \frac{c_j}{6}\left(c_j^2 - 3\,c_j + 2\right)\right) \tag{11}$$

$$a_{2_j} = A_j\left(\Gamma\left(-2 + 3\,c_j\right) - \frac{c_j}{2}\left(-c_j^2 + 2c_j + 1\right)\right) \tag{12}$$

$$a_{3_{j-1}} = A_{j-1}\left(\Gamma\left(1 - 3\,c_j\right) - \frac{c_j}{2}\left(c_j^2 - c_j - 2\right)\right) \tag{13}$$

$$a_{4_{j-2}} = A_{j-2}\left(\Gamma\ c_j + \frac{c_j}{6}\left(c_j^2 - 1\right)\right) \tag{14}$$

$$a_{5_j} = \left(\frac{k_\mathrm{L} f_{d,w}}{h_j^t} + k_\mathrm{s} f_{p,w}\right)\Delta t \tag{15}$$

$$a_{6j} = \left(\frac{k_\mathrm{L}}{h_j\,\mathrm{Kp_b}} + \frac{\alpha}{h_j}\,d_\mathrm{a}\,S_\mathrm{b}\right)\Delta t \tag{16}$$

where k_L, k_s, α, Kp_w, Kp_b, and D_L are all constants, $\Gamma = D_L\,\Delta t \Delta x^{-2}$ is the dimensionless dispersion coefficient and $c_j = U^t_j\ \Delta t\ \Delta x^{-1}$ is the Courant number, Δx is the computational spatial step. The subscript j and superscript t designate spatial and time levels, respectively. Coefficients a_i, A_j, and c_j are time dependent, but superscripts t were omitted for the sake of simplicity.

Equation 4 was discretized according to the following first-order scheme:

$$r_j^{t+1} = r_j^t\left(1 - a_{7_j}\Delta t\right) + C_{Tw_j}^{t+1}\, a_{8_j}\Delta t \tag{17}$$

$$a_{7_j} = \left(\frac{k_L + d_a\,\alpha\,Kp_b\,S_b}{d_a(1 + Kp_bS_b)}\right) \tag{18}$$

$$a_{8_j} = \left(\frac{Kp_b\left(h_j^t\,k_s\,Kp_w\,S_{w_j}^{t+1} + k_L\right)}{d_a\,(1 + Kp_bS_b)\left(1 + Kp_wS_{w_j}^{t+1}\right)}\right) \tag{19}$$

Like Eqs. 3, 5 are discretized as:

$$S_{w_j}^{t+1} = S_{w_j}^t + \frac{1}{A_j}\left(a_{1_j}\,S_{w_{j+1}}^t + a_{2_j}\,S_{w_j}^t + a_{3_j}\,S_{w_{j-1}}^t + a_{4j}\,S_{w_{j-2}}^t\right) - a_{9_j}\,\Delta t \tag{20}$$

In the case of erosive conditions in node j, according to Eq. 6, coefficient a_{9_j} is:

$$a_{9_j} = E_e\left(\frac{\tau_{b_j}^t}{\tau_e} - 1\right) \tag{21}$$

and for deposition conditions, according to Eq. 7, the same coefficient a_{9j} is:

$$a_{9_j} = S_{w_j}^t\lambda\,W_s\left(1 - \left(\frac{U_j^t}{U_{cr}}\right)^2\right) \tag{22}$$

where E_e, λ, W_s, and U_{cr} are constant. Under equilibrium conditions, $a_{9_j} = 0$, and a_{5_j}, a_{6_j}, a_{7_j} and a_{8_j} depend neither on α nor on k_s.

The finite difference Eqs. 10, 17, and 20 are then solved numerically with prescribed initial conditions: $C_{Tw}(x,0)$, $r(0)$, and $S_w(x,0)$; and boundary conditions, in $x=0$: $C_{Tw}(0,t)$ and $S_w(0,t)$. At downstream boundary, in $x = X$: $[\partial C_{Tw}/\partial x]_X = 0$ and $[\partial S_w/\partial x]_X = 0$ are adopted. The calculation sequence begins with S_w, which depends neither on C_{Tw} nor on r.

The assumption of complete mixture in a cross section is adopted for C_{Tw} and S_w, if the point sources are simulated. Therefore, simple balance equations are applied to compute concentration. Though the resulting concentrations C_{Tw} and S_w tend to overestimate the real ones on that particular cross section, the assumption is acceptable for watercourses where the longitudinal spatial scale of transport processes, $E_L = X$, is much higher than the transverse (E_t) and vertical spatial scales (E_v), where $E_t = W$ (river width) and $E_v = h$ (river depth). An estimation of complete mixture length, L_m, can be done from Fischer et al.'s [10] expression for side discharges: $L_m = 0.4\ W^2\ U/\varepsilon_t$, with $\varepsilon_t = k\ u_* h$ transverse diffusion coefficient and k is a constant. Fisher's expression can be applied to straight channels of uniform velocity and conservative substances. In the case of meandering courses, a lower L_m is expected. Likewise, as to temporal scales $T_L >> T_t >> T_v$ should be satisfied, where $T_t = W^2/\varepsilon_t$ is the transverse complete mixture time, $T_v = h^2/\varepsilon_v$ is the vertical complete mixture time and $T_L = X/\tilde{U}$ is travel time, with $\tilde{U}$ stream average velocity and $\varepsilon_v = 0.06\ u_* h$, vertical diffusion coefficient [10].

5 Analytical Solutions

A number of analytical solutions for steady-state flow and different boundary and initial conditions were given by Van Genuchten and Alves [51] for problems with linear adsorption and zero and first-order decay. In order to compare the numerical model predictions with the analytical solutions for the governing Eqs. 3 and 5, a simplified case in the model is assumed; a complete mixture in the cross section was adopted. A chromium and sediment discharge was represented by a planar source at $x=0$. The model and analytical solutions were implemented for a channel 60,000-m long, 45 m in width, and 0.49 m in depth, with a constant rectangular cross section and axe x in the longitudinal direction. A uniform flow $Q = 4.4\ m^3\ s^{-1}$, with velocity $U = 0.20\ ms^{-1}$, Manning coefficient $n = 0.026$, bed slope $S_0 = 0.000073$, $\tau_b = 0.34\ Nm^{-2}$, and $D_L = 10\ m^2\ s^{-1}$ were adopted. These steady flow conditions are similar to those of November, 1999 when the Salado River water level was low. For deposition conditions, the adopted coefficients were: $\lambda = 1$, $U_{cr} = 0.21\ ms^{-1}$, $\tau_e = 0.40\ Nm^{-2}$, $W_s = 0.0001\ ms^{-1}$, and for erosion condition coefficients were: $\tau_e = 0.25\ Nm^{-2}$, $E_e = 0.000001\ kg\ s^{-1}m^{-2}$, and $U_{cr} = 0.04\ ms^{-1}$. The S_w and C_{Tw} longitudinal distributions obtained for deposition, sedimentological equilibrium, and erosion conditions, with $S_w(0,t) = 0.123\ gL^{-1}$, $r(0) = 100\ mg\ kg^{-1}$ and $C_{Tw}(0,t) = 0.287\ g\ L^{-1}$, are shown in Figs. 2, 3, 4, and 5. The parameters used are shown in Table 1. The numerical solutions for S_w given by Eq. 20 and for C_{Tw} given by Eq. 10 are indistinguishable from the analytical results reported by Van Genuchten and Alves [51].

Equation 4 can be written as follows: $\partial r/\partial t = -r\,k_1 + k_2$; it allows the analytic solution shown below, with k_1 and k_2 coefficients:

$$r = \left[(r_0\,k_{10} - k_{20})e^{-k_1 t} + k_2\right]\frac{1}{k_1} \tag{23}$$

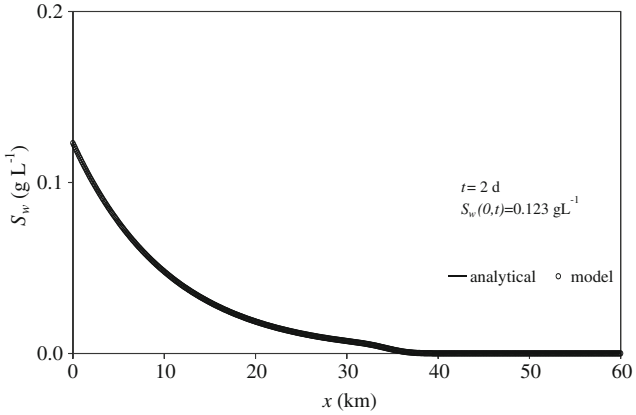

Fig. 2 S_w longitudinal profile comparison. Analytical solution—by van Genuchten and Alves (*solid lines*)—vs. numerical model results (*open dots*) at t=2 days for continuous $S_w(0,t)$, for deposition condition. Distance x measured from upstream boundary section

$$k_1 = \frac{k_L + \alpha\, d_a\, S_b\, Kp_b}{d_a(1 + Kp_b S_b)} \tag{24}$$

$$k_2 = C_{Tw}\left(\frac{Kp_b\,(h\,k_s\,Kp_w\,S_w + k_L)}{d(1 + S_w\,Kp_w)(1 + Kp_b S_b)}\right) \tag{25}$$

with $k_{10}=k_1$ and $k_{20}=k_2(x,0)$.

The r longitudinal distributions obtained for deposition and erosion conditions, with d_a=0.01 m, $r(0)$=100 mg kg^{-1}, $S_w(0,t)$=0.123 g L^{-1}, and $C_{Tw}(0,t)$=0.287 g L^{-1} are shown in Figs. 6 and 7. The model solutions given for r by Eq. 17 were considered satisfactory from the analytical results given by Eq. 23. In this equation, the k_1 and k_2 coefficients are constant, but this mathematical condition was relaxed in order to represent erosion and deposition conditions. Thus, C_{Tw} and S_w were calculated the usual way. A time t=4 days, corresponding to travel time scale, was selected to obtain concentration distributions. Spacial step Δx=100 m and time step Δt=120 s were used to apply the model. The Quickest scheme numerical stability was assured with parameters c= 0.24 and Γ=0.12 [26].

6 Model Implementation

The Salado River headwaters are located in the provinces of Salta and Catamarca (Argentina). It flows over 1,500 km until Santo Tomé town, where it drains into the Paraná River system. The reach under study is about 65.6-km long and belongs to the lower basin (Fig. 8) in Santa Fe province. The average annual flow, at the cross section on provincial route 70 (PR70), is Q=145.6 m^3 s^{-1} [42]. It includes the contribution of the Culúlú Stream basin, with a 3 m^3 s^{-1} average flow. Several towns, such as Esperanza, Franck, and Rafaela, among others, are located in this region which constitutes one of the main milk producing areas in South America, within an important area devoted to agriculture and agribusiness. High concentrations of total dissolved solids (16,000 μS cm^{-1}) were observed. The name of the river, in fact, means "salty." Gallo et al. [11] reported chromium concentrations higher than 8.9 μg L^{-1}, which is the chromium standard value for the protection of aquatic life in freshwater of the Canadian Water Quality Guidelines [5]. The presence of chromium can be attributed to industrial effluent discharges in the surroundings of the 1° de Mayo Channel, on the right side of the Salado River. The effluent discharge was characterized as follows: C_{Tw}= 4.57 mg L^{-1}, S_w=0.030 kg m^{-3}, and flow Q=0.100 m^3 s^{-1}. This source will be referred to onwards as the "discharge." Figure 8 illustrates the extent of the Salado River with the seven sampling sites used in the present work.

The numerical model was implemented in three reaches (see Fig. 8): Salado River, Culúlú Stream, and 1° de Mayo Channel. The first reach extends between cross section 1,

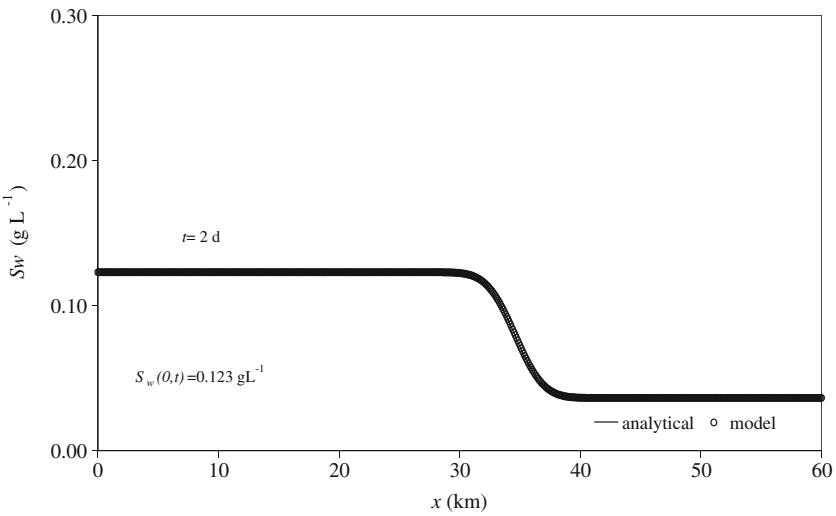

Fig. 3 S_w longitudinal profile comparison. Analytical solution—by van Genuchten and Alves (*solid lines*)—vs. numerical model results (*open dots*) at t=2 days for continuous $S_w(0,t)$, for equilibrium condition. Distance x measured from upstream boundary section

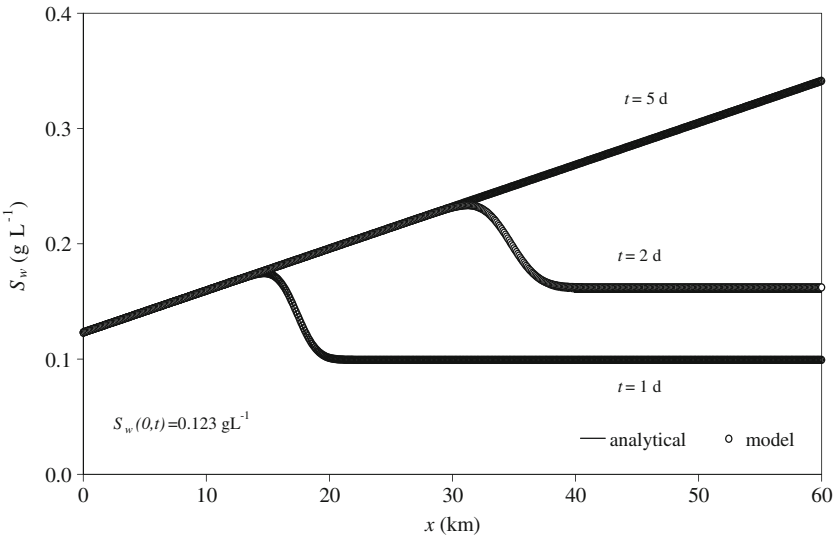

Fig. 4 S_w longitudinal profile comparison. Analytical solution—by van Genuchten and Alves (*solid lines*)—vs. numerical model results (*open dots*) at t=1, 2, and 5 days for continuous $S_w(0,t)$, for erosion condition. Distance x measured from upstream boundary section

upstream boundary, and cross section 2, downstream boundary, located at x=0.0 and x=65.6 km, respectively. Section 1 is 7.7 km upstream from the river intersection with provincial route 6 (PR6), while section 2 is the river intersection with PR70. The second reach stretches along 5.1 km over the Cululú Stream, from section 3, at the intersection with provincial route 50 (PR50), up to its mouth in the Salado River. The third reach corresponds to a stretch of 3.6 km along the 1° de Mayo Channel, between section 4, which defines an upstream boundary, and the channel mouth in the Salado River (section 5), close to the discharge. Other sections, sections 6 and 7, were located 0.3 and 33 km downstream from the discharge (see Fig. 8).

The model was applied to simulate the C_{Tw}, S_w, and r for November 23, when the Salado River flow was low. The river bathymetry was measured in several surveys using a boat equipped with a Raytheon echo sounder and a global positioning system. A sampling from boats and bridges was carried out in order to determine the C_{Tw}, r, and S_w. Each watercourse flow was determined by using an OTT mini-velocimeter: Q=4.61 m^3 s^{-1} in section 1, Q=0.81 m^3 s^{-1} in section 3, and Q=0.10 m^3 s^{-1} in section 4. Surface widths (W) characterizing each watercourse were 30, 14, and 2 m, for the Salado River, Cululú Stream, and 1° de Mayo Channel, respectively, being their corresponding depths 1.50, 0.45, and 0.10 m. Samples were collected at half depth using a Wildco β, 2.2-L horizontal sampling bottle. A Malvern Mastersizer 2000 diffractometer was used to determine suspended sediment granulometry, which showed that 30% were clays (<2 μm), and the remaining were fine silts below 30 μm. In the surroundings of the discharge, chromium bed concentration was r=280 mg kg^{-1} dry weight, for a sample extracted from 1 to 2 cm from the top layer of the bed. More details about field works and laboratory procedures can be found in Gallo et al. [11].

An empirical formula was used to calculate a dispersion coefficient D_L=10.6 m^2 s^{-1} [10]. Spacial and time steps,

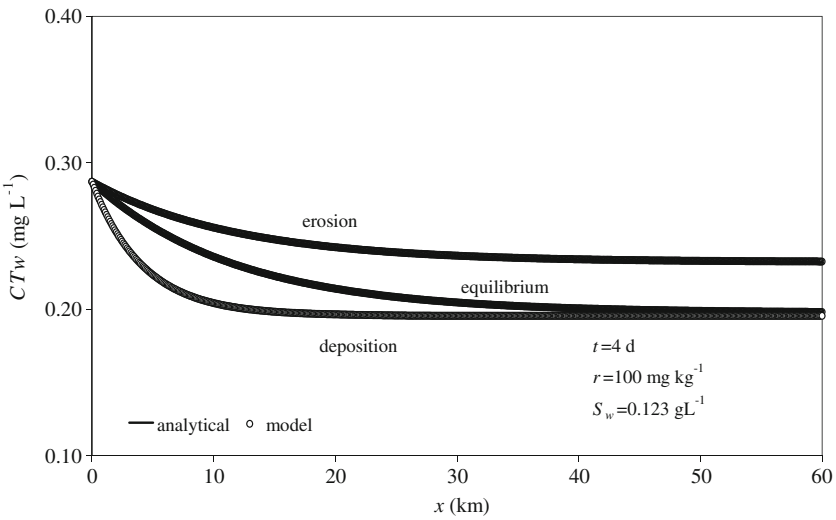

Fig. 5 C_{Tw} longitudinal profile comparison. Analytical solution—by van Genuchten and Alves (*solid lines*)—vs. numerical model results (*open dots*) at t=4 days for continuous C_{Tw} in upstream boundary section, for erosion, deposition, and equilibrium conditions, r=100 mg kg^{-1} and S_w=0.123 g L^{-1}. Distance x measured from upstream boundary section

Table 1 Parameters used in the numerical model and analytical solutions to calculate C_{Tw} and r

k_s 1 s^{-1}	E_e kg $(sm^2)^{-1}$	k_L m s^{-1}	d_a m	Kp_w m^3 kg^{-1}	Kp_b m^3 kg^{-1}	S_b kg m^{-3}
1 10^{-7}	1 10^{-6}	4.910^{-5}	0.01	40	3	1,200

C_{Tw} total metal concentration in water column, r concentration of metal sorbed in bed sediments, k_s deposition rate, E_e empirical constant of erosion, k_L mass transfer coefficient between water column and pore water of bed sediments, d_a active bed sediment layer, Kp_w partition distribution coefficient in the water column, Kp_b partition distribution coefficient in bed sediments, S_b sediment concentration in the bed environmental volume

Δx=100 m and Δt=120 s, respectively, were adopted in accordance with both result requirements and numerical scheme stability conditions (Leonard, 1979). Settling velocity, W_s, was set at 0.0001 m s^{-1}, which is an appropriate assumption for suspended silt and clay granulometry. As to initial conditions and based on the data collected, the following values were considered: $C_{Tw}(x,0)$=0.002 mg L^{-1}, $r(0)$=10 mg kg^{-1}, and $S_w(x,0)$=0.0364 kg m^{-3}. Table 2 shows the upstream boundary conditions for $C_{Tw}(0,t)$ and $S_w(0,t)$ measured in sections 1, 3, and 4.

Partition coefficient was set taking into account a mean value, Kp_w=40.0 m^3 kg^{-1}, from a detailed analysis by [11]. The bed sediment density was computed from the bed porosity, which was 0.50<ϕ<0.62, therefore, an S_b= 1,200 kg m^{-3} average was determined. Others parameters k_s=1.00 10^{-7} s^{-1}, λ=1.0, E_e=1 10^{-6} kg s^{-1} m^{-2}, and d_a= 0.01 m were adopted [8]. In the model calibration, Kp_b= 3.00 m^3 kg^{-1}, k_L=4.95 10^{-5} m s^{-1}, U_{cr}=0.081 m s^{-1}, τ_e= 0.26 N m^{-2}, were treated as model parameters for the Salado River that must be adjusted to match the measured concentrations. τ_e=0.35 N m^{-2} was adopted for the other watercourses. The critical shear stresses for erosion were selected taking into account both bibliography [19] and bed sediment granulometry [25]. A dynamic viscosity μ was calculated with a state equation, as a function of temperature [6].

7 Results and Discussion

Gradually varied unsteady flow was calculated with the HEC-RAS 4.0 system [3] for a time interval from October 23, 1999 to February 13, 2000. The flow was characterized by average velocities between 0.08 and 0.30 m s^{-1} for the Salado River, 0.20 m s^{-1} for the Cululú Stream and 0.10 m s^{-1} for the 1° de Mayo Channel. Flow and water gauge were 4.66<Q<5.76 m^3 s^{-1} and 0.26<h<0.87 m, respectively at the control section on PR70. The distance required for complete mixing from the right side discharge was L_m≈2,700 m, that is L_m << X, with ε_t=0.045 m^2 s^{-1}. Temporal scale values were: T_L=122 h, T_t=12 h, and T_h= 1.5 h (with ε_v=0.0030 m^2 s^{-1}), which shows T_L >> T_t >> T_v. These results allow us to accept the conditions of near-instantaneous mixing in the vertical direction and relatively rapid mixing in the transverse direction, basic requirements for implementing a one-dimensional transport model. Figure 9 shows the plume resulting from the discharge on the right riverbank. The photograph, taken on November 23, 1999 shows that the plume reaches approximately the center of the section and disperses downstream, without mixing completely at the cross section.

The spatial variations of C_{Tw} along the stream are represented in Fig. 10. The comparison of measured and predicted C_{Tw} is also presented. Results show that chromium

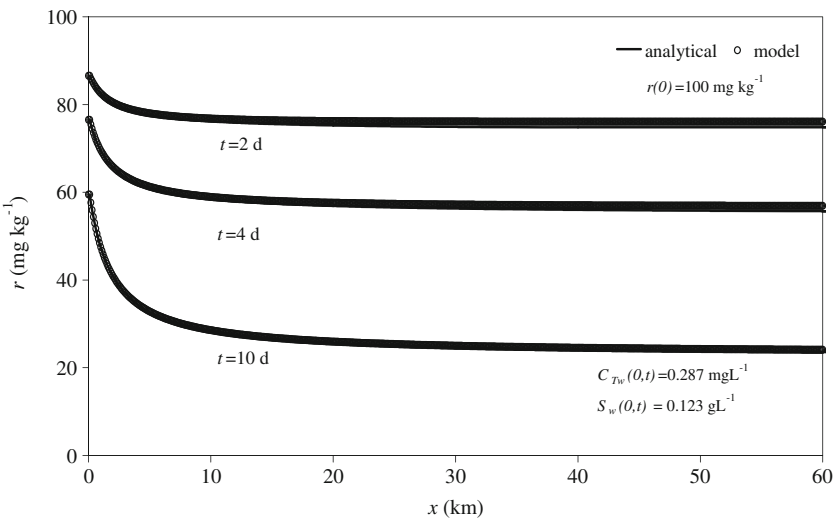

Fig. 6 r longitudinal profile comparison. Analytical solution of Eq. 23 (*solid lines*) vs. numerical model results (Eq. 17) (*open dots*) at t=2, 4, and 10 days, for erosion condition, with $r(0)$=100 mg kg^{-1}, $C_{Tw}(0,t)$=0.287 mg L^{-1} and $S_w(0,t)$=0.123 g L^{-1}. Distance x measured from upstream boundary section

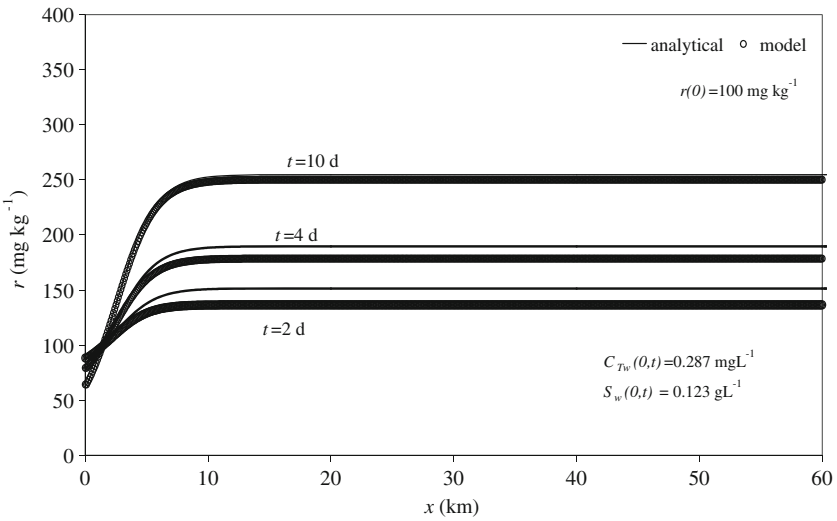

Fig. 7 r longitudinal profile comparison. Analytical solution of Eq. 23 (*solid lines*) vs. numerical model results (Eq. 17) (*open dots*) at t=2, 4, and 10 days, for deposition condition, with $r(0)$=100 mg kg^{-1}, $C_{Tw}(0,t)$=0.287 mg L^{-1} and $S_w(0,t)$=0.123 g L^{-1}. Distance x measured from upstream boundary section

discharge, located at x=7.6 km, produces a local impact with a peak C_{Tw}=0.101 mg L^{-1} at x=7.8 km. This concentration is tenfold higher than $C_{Tw}(0,t)$=0.010 mg L^{-1}. The distribution of chromium computed downstream the discharge, which shows a constant declining trend up to x=50 km. Further downstream, the distribution of chromium decreased continuously, but with local variations, to the downstream section of the reach, PR70. The Cululú Stream water input, which occurs at x=3.7 km, does not show relevance for the chromium-studied conditions in the Salado River. Therefore, the transport process was under discharge control.

The chromium concentration in the bottom sediments behaves in different ways regarding the water column. Figure 11 shows the longitudinal profile of the computed r in t=30 days and r measured at sampling sections 1, 6, 7, and 2. The initial condition $r(0)$=10 mg kg^{-1} increased in one order of magnitude near the discharge section. A decreasing gradient is observed up to x=40 km for the r longitudinal profile. Then, between 40 and 55 km, the decreasing trend is slightly greater, and from 55 to 60 km there is a very noticeable negative gradient. From that point onwards, r becomes stable. The maximum is reached with r=88.9 mg kg^{-1} at x=8.1 km, immediately downstream of the source.

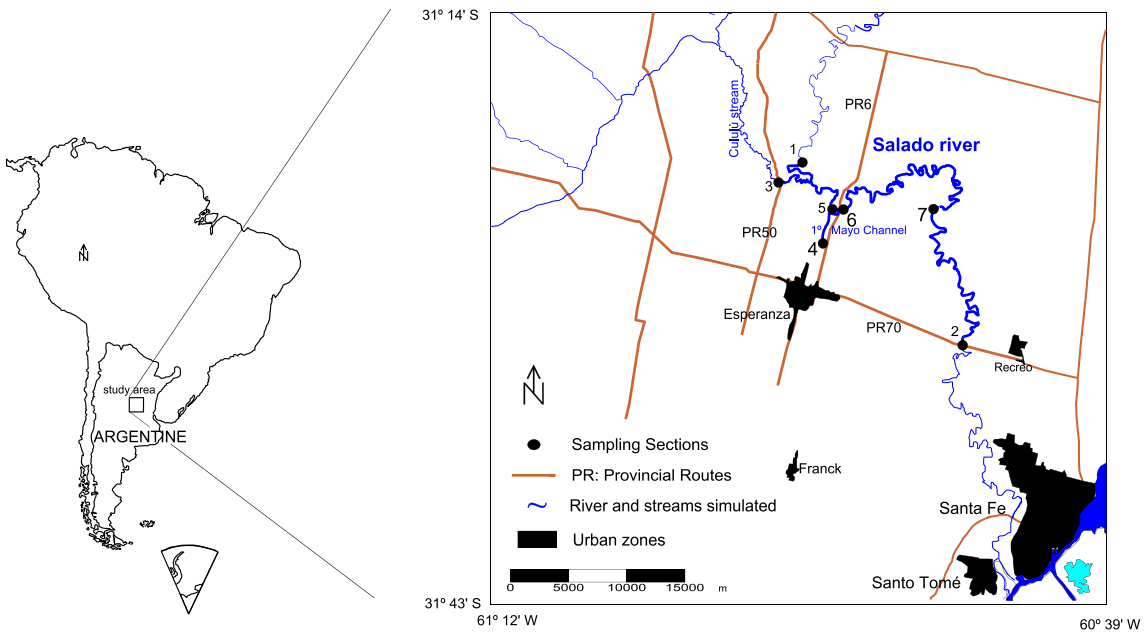

Fig. 8 Maps showing the location of the Salado River, the Cululú Stream, and the 1° de Mayo Channel and the seven sampling sites

Table 2 S_w and C_{Tw} upstream boundary conditions for Salado River, Cululú Stream, and 1° de Mayo Channel for model simulation on November 23, 1999

	Cross section	S_w (0,t) (kg m^{-3})	C_{Tw} (0,t) (mg L^{-1})
Salado River	1	0.125	0.010
Cululú Stream	3	0.030	0.017
1° de Mayo Channel	4	0.020	0.030

S_w sediment concentration in the water column, C_{Tw} total metal concentration in water column

Figure 12 represents the S_w longitudinal profile calculated and measured along the river. The concentrations shows a general slow declining trend up to x=40 km, and it remains almost constant with slight local variations, corresponding to sedimentological equilibrium conditions. From x=20 km to x=50 km, the τ_b values are between 0.144 and 0.069 N m^{-2}, then between 56 km<x<63 km, τ_b slightly exceeds τ_e. The highest τ_b=0.60 N m^{-2} is calculated at x=58 km. The time scale of the fine sediment transport is about 7 days, which relates to travel time, T_L=5.1 days, which in turn is equivalent to an advective time scale.

The sensitivity of the model regarding changes in the initial conditions was analyzed. The results showed the importance of the initial conditions for the spatial distribution of r and the low relevance for S_w and C_{Tw}. The observation is justified in that the last two variables required a time similar to the travel time to be compared with the measurements, whereas for r, a substantially higher temporal scale was required. The profiles calculated for S_w, C_{Tw}, and r were fitted to the measurements. For the first two variables, the best fit is achieved for t=8 days, and for r, the best fit was performed for t=30 days. This is compatible with works by other authors [7, 18].

For the conditions of model implementation, it was observed that over the 40 days prior to measurements, the flow variations were ±11% the flow gauged on November 23, 1999. Therefore, it can be stated that the flow was unsteady, gradually varied, with slight temporal variations.

The particulate fraction in the water column, $f_{pw}=S_w Kp_w/(1+S_w Kp_w)$, was higher than the dissolved one $f_{dw}=1/(1+S_w Kp_w)$ along almost all the reach. The f_{pw} was determined from S_w and Kp_w. The former was calculated with the model, and the latter was determined by Gallo et al. [11]. The average f_{pw} was about 0.66.

A relevant parameter was the active layer depth, since the greater the d_a, the slower the changes of C_{Tw} and r. For example, for the same case analyzed, when d_a=3 cm was adopted, the transport processes were slower for C_{Tw} and r. The calculated r longitudinal profile showed less variation, mainly near the source. Therefore, r corresponds to higher time scales, as it was reported by Chen et al. [7]. Both the deposition and erosion thickness calculated were <1 mm along the reach for t=30 days, then, the assumptions S_b and d_a constant can be accepted.

The results obtained for r applying Eq. 23 show an error of 16% regarding those calculated by Eq. 17. The overestimation for the analytical solution may have been due to the fact that neither C_{Tw} nor S_w were kept constant. The salinity effect on the partition coefficient [45] was not

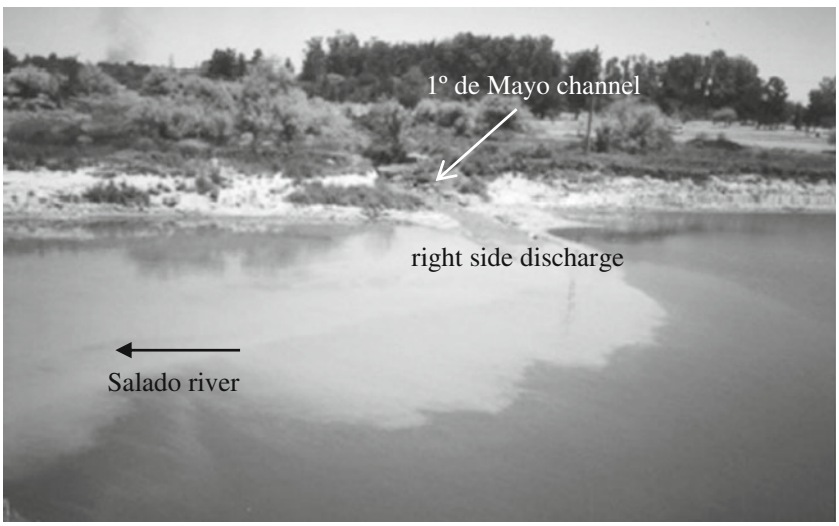

Fig. 9 Section 5 at Salado River and 1° de Mayo Channel mouth. Plume resulting from the right side discharge: C_{Tw}= 4.57 mg L^{-1}, S_w=0.030 kg m^{-3}, and Q=0.100 m^3 s^{-1}

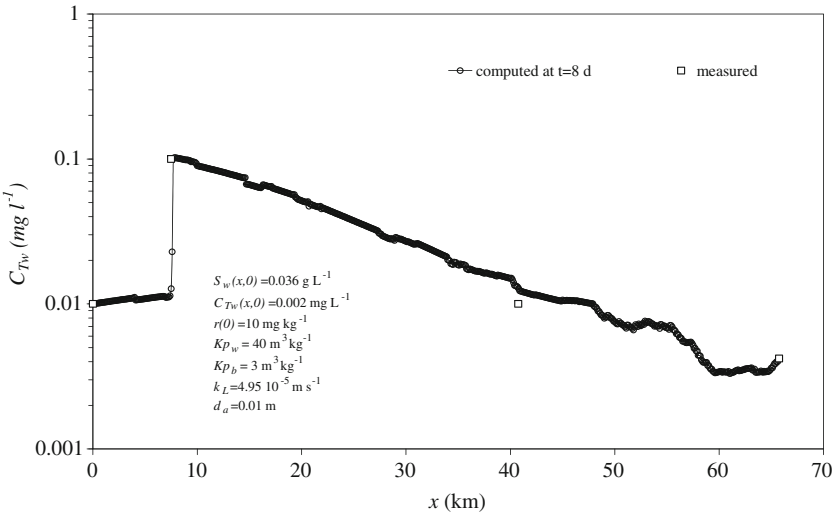

Fig. 10 Comparison of measured and predicted $C_{T,w}$ longitudinal profiles at t=8 days. Distance x measured from section 1 in the Salado River. Chromium discharge is located at x=7.6 km

analyzed because changes in salinity were negligible for the analyzed conditions.

8 Conclusions

A three-equation mathematical model was developed to represent the chromium exchange process between the bed and the water column, considering metal sorption kinetics for instantaneous equilibrium conditions, as well as the mechanical processes of erosion/deposition of fine sediments.

The differential equations for C_{Tw} and S_w of the mathematical model were approximated by the Quickest numeric scheme. r was calculated with a simple scheme in finite differences. Numerical vs. analytical solutions for C_{Tw}, r and S_w under erosion/deposition and equilibrium conditions were considered satisfactory.

The longitudinal profiles calculated by the model for C_{Tw}, r, and S_w in the reach of 65.6-km long of the Salado River showed a good fit to the measurements. The model properly represents the impact of the discharge into the river, increasing C_{Tw} from 0.01 mg L^{-1} to 0.1 mg L^{-1} and r from 6 mg kg^{-1} to 100 mg kg^{-1}.

Chromium concentrations, C_{Tw} and r, were mainly controlled by the discharge concentrations for the low-flow conditions studied. The calculated time scale for C_{Tw} and S_w were 8 days being associated to travel time, whereas the r scale was 30 days. The active layer thickness, d_a, was an important parameter, mainly for r time scale. The chromium particulate fraction in the water column shows the importance of studying the association of chromium with sediments.

A greater number of field measurements and laboratory tests would also allow better parameter calibration, particu-

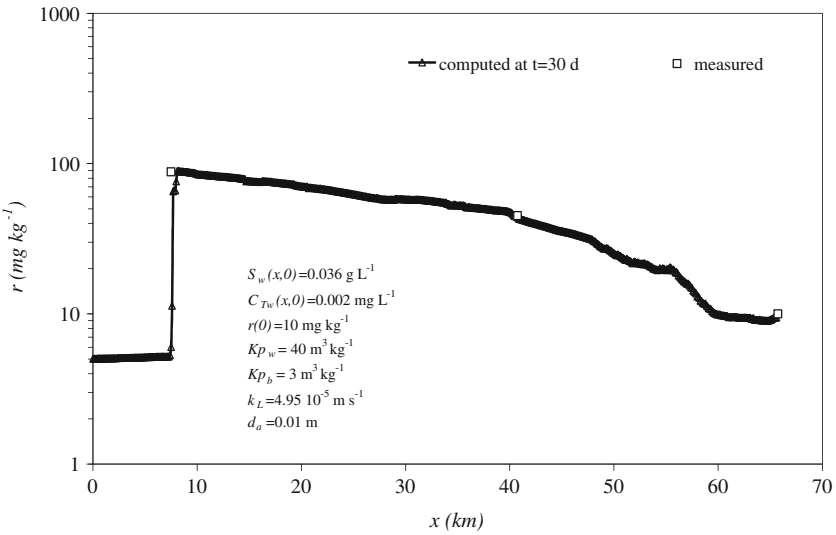

Fig. 11 Comparison of measured and predicted r longitudinal profiles at t=30 days. Distance x measured from section 1 in the Salado River. Chromium discharge is located at x=7.6 km

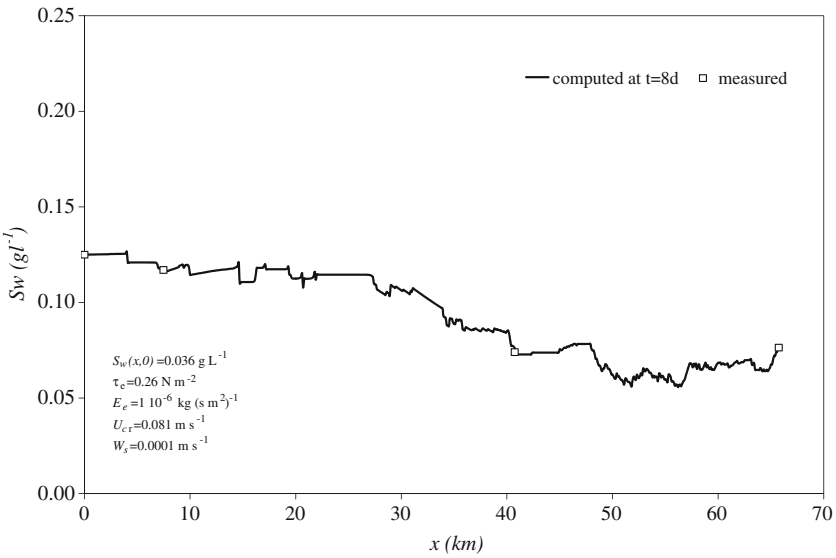

Fig. 12 Comparison of measured and predicted S_w profiles at t=8 days in the Salado River. Distance x measured from section 1 in the Salado River

larly for d_a, Kp_b, and k_L. It would also be possible to model other environmental situations.

Acknowledgments This work was supported by Universidad Nacional del Litoral (project CAI+D 2009 PI 38–194) and by Agencia Nacional de Promoción Científica y Tecnológica (project PICT Raices 35885).

Appendix: Nomenclature

A [m^2]	Cross section area
c_j	Courant number
C_{pb} [kg$_{HM}$ m^{-3}]	Particulate metal concentration in the bed
C_{pw} [kg$_{HM}$ m^{-3}]	Particulate metal concentration in water column
C_{sb} [kg$_{HM}$ m^{-3}]	Soluble metal concentration in the bed
C_{sw} [kg$_{HM}$ m^{-3}]	Soluble metal concentration in water column
C_{Tw} [kg$_{HM}$ m^{-3}]	Total metal concentration in the water column
d_a [m]	Active bed sediment layer
D_L [m^2 s^{-1}]	Longitudinal dispersion coefficient
E [m^{-1}]	Vegetation trapping efficiency per unit distance
E_e [kg m^{-2} s^{-1}]	Erosion empirical constant
E_L	Longitudinal spatial scale of transport processes
E_t	Transverse spatial scale of transport processes
E_v	Vertical spatial scale of transport processes
f_{dw}	Dissolved fraction in water column
f_{pw}	Particulate fraction in water column
g [m s^{-2}]	Gravitational acceleration
h [m]	Water column depth
k	Dimensionless constant (transverse diffusion coefficient equation)
k_L [m s^{-1}]	Mass transfer coefficient
Kp_b [m^3 kg^{-1}]	Partition or distribution coefficient in the bed
Kp_w [m^3 kg^{-1}]	Partition or distribution coefficient in the water column
k_s [s^{-1}]	Deposition rate
k_1, k_{10} [s^{-1}]	Coefficient
k_2, k_{20} [kg$_{HM}$ kg^{-1} s^{-1}]	Constant coefficient
L_m [m]	Complete mixture length
m_d [kg m^{-2} s^{-1}]	Sediment deposition rate
m_e [kg m^{-2} s^{-1}]	Sediment erosion rate
n [s m$^{-1/3}$]	Manning coefficient
p	Proportion of the water column occupied by vegetation
Q [m^3 s^{-1}]	Stream flow
q [m^2 s^{-1}]	Floodplain unit flow in the x direction
R [m]	Hydraulic radius
r [kg$_{HM}$ kg^{-1}]	Concentration of metal sorbed in bed sediments
S_b [kg m^{-3}]	Sediment concentration in the bed environmental volume
S_0 [m m^{-1}]	Bed slope
S_w [kg m^{-3}]	Total suspended sediment concentration
T_L [s^{-1}]	Travel time/longitudinal temporal scale
T_t [s^{-1}]	Transverse temporal scale
T_v [s^{-1}]	Vertical temporal scale
t [s]	Time coordinate

U [m s^{-1}]	Mean velocity in the cross section
U_{cr} [m s^{-1}]	Critical velocity sediment deposition
$\tilde{U}$ [m s^{-1}]	Stream average velocity
u_* [m s^{-1}]	Friction velocity
W [m]	River width
W_s [m s^{-1}]	Settling velocity
x [m]	Longitudinal coordinate
α [s^{-1}]	Resuspension/erosion rate
Δx [m]	Computational spatial step
Δt [s]	Computational time step
ε_t [m^2 s^{-1}]	Transverse diffusion coefficient
ε_v [m^2 s^{-1}]	Vertical diffusion coefficient
$\gamma = h/d_a$	Dimensionless coefficient
λ	Dimensionless deposition constant
Γ	Dimensionless dispersion coefficient
$\emptyset$	Bed porosity
ρ_s [kg m^{-3}]	Mass density of sediment grains
ρ_w [kg m^{-3}]	Water density
τ_e: [N m^{-2}]	Erosion critical shear stress

References

1. Ariathurai, R., & Arulanandan, K. (1978). Erosion rates of cohesive soils. *Journal of Hydraulics Division, 104*, 279–283.
2. Beltrame, M., De Marco, S., & Marcovecchio, J. (2009). Dissolved and particulate heavy metals distribution in coastal lagoons. A case study from Mar Chiquita Lagoon, Argentina. *Estuarine, Coastal and Shelf Science, 85*, 45–56.
3. Bruner, G. (2008). HEC RAS, River Analysis System User's Manual, v. 4.0, U.S. Army Corps of Engineers. http://www.hec.usace.army.mil. Accessed 16 April 2008.
4. Bryan, G., & Langston, W. (1991). Bioavailability, accumulation and effects of heavy metals in sediments with special reference to United Kingdom estuaries: a review. *Journal of Environmental Pollution, 131*, 76–89.
5. CCME. (1999). *Canadian Council of Ministers of the Environment, Canadian Water Quality Guidelines for the Protection of Aquatic Life: chromium-hexavalent chromium and trivalent chromium*. Winnipeg: Canadian Council of Ministers of the Environment.
6. Chapra, S. (1997). *Surface water-quality modelling*. Iowa: Wiley.
7. Chen, C., Leva, D., & Olivieri, A. (1996). Modeling the fate of copper discharged to San Francisco Bay. *Journal of Environmental Engineering, 122*(10), 924–934.
8. Di Toro, D. M. (2001). *Sediment flux modeling*. New York: Wiley.
9. Fairbrother, A., Wenstel, R., Sappington, K., & Wood, W. (2007). Framework for metals risk assessment. *Ecotoxicology and Environmental Safety, 68*, 145–227.
10. Fischer, H. B., List, E. J., Koh, R. C. Y., Imberger, J., & Brooks, N. H. (1979). *Mixing in inland and coastal waters*. New Mexico: Hermosa Publ.
11. Gallo, M., Trento, A., Alvarez, A., Beldoménico, H., & Campagnoli, D. (2006). Dissolved and particulate heavy metals in the Salado river (Santa Fe, Argentina). *Water, Air, and Soil Pollution, 174*, 367–384.
12. Gagnon, C., & Saulnier, I. (2003). Distribution and fate of metals in the dispersion plume of a major municipal effluent. *Environmental Pollution, 124*, 47–55.
13. Gibbs, R. (1983). Effect of natural organic coatings on the coagulation of particles. *Environmental Science & Technology, 17*(4), 237–240.
14. Hartnett, M., & Berry, A. (2010). Transport of lead in the Mersey Estuary: the development of a novel approach to deriving partition coefficients. *Advances in Engineering Software, 41*, 84–91.
15. Hayter, J., & Pakala, C. V. (1989). Transport of inorganic contaminants in estuarial waters. *Journal of Coastal Research, 5*, 217–230.
16. Huang, S. (2001). Cadmium adsorption by sediment in a turbulent tank. *Water Research, 35*(11), 2635–2644.
17. Jackman, A., Kennedy, V., & Bathia, N. (2001). Interparticle migration of metal cations in stream sediments as a factor in toxics transport. *Journal of Hazardous Mateterials, 82*(1), 27–41.
18. Ji, Z., Hamrick, J., & Pagenkopf, J. (2002). Sediment and metals modeling in shallow river. *Journal of Environmental Engineering, 128*(2), 105–119.
19. Jiang, J., & Mehta, A. (2001). Fine-grained sedimentation in a shallow harbor. *Journal of Coastal Research, 17*(2), 389–393.
20. Johansson, H., Lindstrom, M., & Hakanson, L. (2001). On the modelling of the particulate and dissolved fractions of susbstances in aquatic ecosystems-sedimentological and ecological interactions. *Ecological Modelling, 137*, 225–240.
21. Karvelas, M., Katsoyiannis, A., & Samara, C. (2003). Occurrence and fate of heavy metals in the wastewater treatment process. *Chemosphere, 53*(10), 1201–1210.
22. Katopodes, N., & Piasecki, M. (1996). Site and size optimization of contaminant sources in surface water systems. *Journal of Environmental Engineering, 122*(10), 917–934.
23. Kimbrough, D., Cohen, Y., Winer, A., Creelman, L., & Mabuni, C. (1999). A critical assessment of chromium in the environment. *Science and Technology, 29*(1), 1–46.
24. Krank, K., & Milligan, T. (1992). Characteristics of suspended particles at an 11-hour anchor station in San Francisco Bay, California. *Journal of Geophysical Research, 97*, 11373–11382.
25. Kröhling, D., & Orfeo, O. (2002). Sedimentología de unidades loéssicas (Pleistoceno Tardío-Holoceno) Del Centro-Sur De Santa Fe. *Revista de la Asociación Argentina de Sedimentología, 9*(2), 135–154.
26. Leonard, B. (1979). A stable and accurate convective modelling procedure based on quadratic upstream interpolation. *Computational Methods in Applied Mechanics and Engineering, 19*, 59–98.
27. Maddock, J., & Lópes, C. (1988). Behaviour of pollutant metals in aquatic sediements. In U. Seelinger, L. Lacerda, & S. Patchineelam (Eds.), *Metals in coastal environments of Latin America* (pp. 100–105). Heidelberg: Springer.
28. Manning, A., & Bass, S. (2006). Variability in cohesive sediment settling fluxes: observations under different estuarine tidal conditions. *Marine Geology, 235*, 177–192.
29. Marcovecchio, J., & Ferrer, L. (2005). Distribution and geochemical partitioning of heavy metals in sedimentos of the Bahía Blanca Estuary, Argentina. *Journal of Coastal Research, 21*(4), 826–834.
30. Markofsky, M., & Westrich, B. (2007). Transport modeling. In B. Westrich & U. Forstner (Eds.), *Sediment dynamics and pollutant mobility in rivers, an interdisciplinary approach* (pp. 117–169). Berlin: Springer.
31. Mehta, A. (1989). On estuarine cohesive sediment behaviour. *Journal of Geophysical Research, 94*(C10), 14303–14314.
32. Mwanuzi, F., & De Smedt, F. (1999). Heavy metals distribution model under estuarine mixing. *Hydrological Processes, 13*(5), 789–804.
33. Ng, B., Turner, A., Tyler, A., Falconer, R., & Millward, G. (1996). Modelling contaminant geochemistry in estuaries. *Water Research, 30*(1), 63–74.

34. Ng, S., Wai, O., Li, Y., Li, Z., & Jiang, Y. (2009). Integration of a GIS and a complex three-dimensional hydrodynamic, sediment and heavy metal transport numerical model. *Advances in Engineering Software, 40*, 391–401.
35. Nicholas, A., Walling, D., Sweet, R., & Fang, X. (2006). New strategies for upscaling high-resolution flow and overb ank sedimentation models to quantify floodplain sediment storage at the catchment scale. *Journal of Hydrology, 329*, 577–594.
36. Paterson, D., Tolhurst, T., Kelly, J., Honeywill, C., de Deckere, E., Huet, V., et al. (2000). Variations in sediment properties, Skeffing mudflat, Humber Estuary, UK. *Continental Shelf Research, 20*, 1373–1396.
37. Periáñez, R. (2009). Environmental modelling in the Gulf of Cadiz: heavy metal distributions in water and sediments. *The Science of the Total Environment, 407*, 3392–3406.
38. Schnoor, J. L. (1996). Environmental modeling. Fate and transport of pollutants in water air and soil. In J. Schnoor & A. Zehnder (Eds.), *Modelling trace metals* (pp. 381–483). Iowa: Wiley.
39. Shrestha, P., & Orlob, G. (1996). Multiphase distribution of cohesive sediments and heavy metals in estuarine systems. *Journal of Environmental Engineering, 112*(8), 730–740.
40. Sin, S., Chua, N., Lo, W., & Ng, L. (2001). Assessment of heavy metal cations in sediments of Shing Mun River, Hong Kong. *Environmental International, 26*(5–6), 297–301.
41. Singh, A., Hasnaiun, S., & Banerjee, D. (1999). Grain size and geochemical partitioning of heavy metals in sediments of the Damodar River—a tributary of the Lower Ganga, India. *Enviromental Geology, 39*(1), 90–98.
42. SSRHN (2004). *Estadística Hidrológica del Siglo XX*. Subsecretaría de Recursos Hídricos Presidencia de la Nación. Rep. Argentina.
43. Thomann, R. V., & Mueller, J. A. (1987). *Principles of surface water quality modeling and control*. New York: Harper Collins Publishers.
44. Turner, A., & Millward, G. (1994). Partitioning of trace-metal in a macrotidal estuary. Implications for contaminant transport models. *Estuarine, Coastal and Shelf Science, 39*, 45–58.
45. Turner, A. (1996). Trace-metal partitioning in estuaries: importance of salinity and particle concentration. *Marine Chemistry, 54*, 27–39.
46. Turner, A. (2000). Trace metal contamination in sediments from U.K. Estuaries: an empirical evaluation of the role of hydrous iron and manganese oxides. *Estuarine, Coastal and Shelf Science, 50*, 355–371.
47. USDHHS. (2004). U.S. Department of Health and Human Services, Public Health Service, National Toxicology Program. Report on Carcinogens, Eleventh Edition. Chromium Hexavalent Compounds. Program Section 301(b) (4) of the Public Health Service Act as Amended by Section 262, PL 95–622. http://ntp.niehs.nih.gov/ntp/roc/toc11.html. Accessed 3 Nov 2004.
48. USEPA. (1984). U.S. Environmental Protection Agency. Technical guidance manual for performing wasteload allocations, Book II: Stream and rivers. http://www.epa.gov/waterscience/pc/watqual.html. Accessed 3 Oct 2002.
49. USEPA. (1999). U.S. Environmental Protection Agency. Office of Air and Radiation. *Understanding variation in partition coeffi-cient values, Volume I: The Kd model methods of measurement, and application of chemical reaction codes*. Retrieved from: http://www.epa.gov/radiation/cleanup/402-r-99-004.html#vol1. Accessed October 3, 2002.
50. USEPA. (1999). U.S. Environmental Protection Agency. Office of Solid Waste. Partition coefficients for metals in surface water solid and waste. http://www.epa.gov/epaoswer/hazwaste/id/hwirwste/pdf/risk/reports/0524.pdf. Accessed 15 Oct 2002.
51. van Genuchten, M. T., & Alves, W. J. (1982). *Analytical solutions of the one-dimensional convective-dispersive solute transport equation. Technical Bulletin 1661*. Washington, D.C.: US Department of Agriculture.
52. Wang, F., & Chen, J. (2000). Relation of sediment characteristics to trace metal concentration: a statistical study. *Water Research, 34*(2), 694–698.
53. Wen, X., & Allen, H. (1999). Mobilization of heavy metals from Le An River sediment. *The Science of the Total Environment, 227*, 101–108.
54. Wen-Cheng, L., Shu-Wei, C., Kuo-Tung, J., Liang-Saw, W., & Kon-Kee, L. (2007). Modelling diagnosis of heavy metal (copper) transport in an estuary. *The Science of the Total Environment, 388*, 234–249.
55. Westrich, B., & Förstner, U. (2007). *Sediment dynamics and pollutant mobility in rivers, an iinterdisciplinary approach*. Berlin: Springer.
56. Winterwerp, J. C., & Kesteren, W. G. M. (2004). *Introduction to the physics of cohesive sediment in marine environment*. Amsterdam: Elsevier.
57. Wu, Y., Falconer, R., & Lin, B. (2005). Modelling trace metal concentration distributions in estuarine waters. *Estuarine, Coastal and Shelf Science, 64*, 699–709.
58. Zagar, D., Knap, A., Warwick, J., Rajar, R., Horvat, M., & Cetina, M. (2006). Modelling of mercury transport and transformation processes in the Idrijca and Soca river system. *The Science of the Total Environment, 368*(1), 149–163.
59. Zago, C., Giblin, A., & Bergamasco, A. (2001). Changes in the metal content of superficial sediments of Boston Harbor since the cessation of sludge discharge. *Marine Environmental Research, 51*(5), 389–415.
60. Zhaohui, W., & Huang, S. (1999). Environmental hydraulics. In J. Lee, A. W. Jayawardena, & Z. Wang (Eds.), *Effect of sediment on pollutant transport-transformation* (pp. 713–722). China: Hong Kong.